Corrosion Science 198 (2022) 110111

Contents lists available at ScienceDirect

Corrosion Science

journal homepage: www.elsevier.com/locate/corsci

The contribution of Zn(II) and phosphate anions to the inhibition of organic coating cathodic disbondment on galvanised steel by zinc phosphate pigment

C.M. Griffiths *, N. Wint, G. Williams, H.N. McMurray

Materials Research Centre, College of Engineering, Swansea University, Bay Campus, Fabian Way, Crymlyn Burrows, Swansea SA1 8EN, UK

ARTICLE INFO

Keywords:
A: metal coatings
Organic coatings
Zinc
C: Atmospheric corrosion
Paint coatings
Polymer coatings

ABSTRACT

In-situ scanning Kelvin probe (SKP) measurements are used to investigate the relative contributions of in-coating zinc (II) cations and phosphate anions to the inhibition of corrosion-driven cathodic disbondment by zinc phosphate (ZnPhos) pigments. Using hot-dip galvanized steel (HDG) substrates, delamination rates of model polyvinylbutyral (PVB) coatings comprising different pigment volume fractions (ϕ) of phosphate-loaded hydrotalcite and Zn(II)-exchanged bentonite are compared with those established in the presence of ZnPhos. The most powerful inhibitory effect is obtained using in-coating Zn^{2+}, while ZnPhos pigments inhibit cathodic disbondment rather weakly and as such the principal function of phosphate is to control Zn^{2+} solubility.

1. Introduction

Organically coated hot dipped galvanised steel (HDG) is commonly used in the automotive and construction industries [1]. These organic coatings are multi-layered and consist of a conversion coating, primer, and topcoat. Conversion coatings are applied to the HDG substrate surface and provide corrosion protection and improved adhesion for the primer layer [2]. The primer contains polymeric binders and fillers which provide barrier protection to moisture and corrosive species, and corrosion inhibitor pigments that provide active corrosion protection [1]. The topcoat provides aesthetics and further barrier protection. A common failure mechanism relevant to organically coated zinc substrates is that of corrosion driven cathodic disbondment [1] where a corrosion cell is established when corrosive electrolyte contacts the metal substrate at a coating defect. Here, the electrolyte acts to couple anodic metal dissolution at the organic coating defect, with cathodic oxygen reduction at the adjacent coating-metal interface. The mechanism of organic coating disbondment has been postulated to occur due to intermediate products of the oxygen reduction reaction, such as HO_2^- and H_2O_2, and that the resultant alkaline underfilm environment promotes zinc (hydr)oxide dissolution, polymer degradation and hydrolysis of interfacial bonds at the cathodic site [3–7].

Corrosion inhibitor pigments based on sparingly soluble salts such as strontium chromate ($SrCrO_4$), are known to provide excellent corrosion resistance when used within the primer layer of organic coatings [8–12]. Strontium chromate and other hexavalent chromium based pigments have been found to be toxic and carcinogenic, which has meant that alternative, safe inhibitor pigments have been developed [13,14]. Zinc phosphate (ZnPhos) is a sparingly soluble salt which is used as an alternative to chromate-based inhibitor pigments and is the current industrial standard for use in organic coatings [1]. However, the inhibition efficiency afforded by ZnPhos has been reported to be limited due to its low solubility (($Zn_3(PO_4)_2$, $K_{sp} = 9 \times 10^{-33}$ mol^3 dm^{-9}) [10,15–24]. Wint et al. [25] showed that ZnPhos dispersed in a polyvinyl butyral coating on HDG was only able to reduce the rate of cathodic disbondment by 66% compared to an unpigmented coating, while strontium chromate completely prevented cathodic disbondment over a 24 h period in a similar study by Williams et al. [9] using the same model organic coating and substrate. Mousavifard et al. [26] showed that ZnPhos, present within an epoxy coating, dissociated into its constituent ions via reaction (1) when the coated HDG steel was subjected to aqueous sodium chloride solution via salt spray testing.

$$Zn_3(PO_4)_{2(s)} \rightleftharpoons 3Zn^{2+}{}_{(aq)} + 2PO_4^{3-}(aq) \quad (1)$$

Whilst it is assumed that the principal function of ZnPhos inhibitive pigments is to act as a store of PO_4^{3-} ions, which leach out from an organic coating to provide corrosion inhibition at defect sites, the role the associated Zn^{2+} cations is not so apparent. There is evidence that in-

* Corresponding author.
E-mail address: c.m.griffiths@swansea.ac.uk (C.M. Griffiths).

https://doi.org/10.1016/j.corsci.2022.110111
Received 22 October 2021; Received in revised form 13 January 2022; Accepted 19 January 2022
Available online 21 January 2022

coating Zn^{2+} cations can act to significantly retard the rate of corrosion-driven organic coating cathodic delamination on metallic zinc based substrates [27]. In this work we seek to compare the efficiency of the constituent ions of ZnPhos separately by employing ion-exchange or "smart-release" pigments and comparing their performance with an industry standard ZnPhos sparingly soluble pigment. Ion-exchange pigments can be exchanged with either cationic or anionic species and have been used to investigate the effect of particular ionic species on corrosion mechanisms such as cathodic disbondment [28–30]. A benefit of using ion-exchange pigments over sparingly soluble salts is their ability to only release stored inhibitive species when the pigment encounters a corrosive ionic species, such as Cl^-, which they then sequester. In contrast, sparingly soluble salts will continuously leach their constituent ions when in contact with an electrolyte, reducing the long term corrosion inhibition efficiency of the coating [11,31].

An example of an cation-exchange material is bentonite clay, a form of montmorillonite, which has pH independent cationic exchange properties [32–36]. The use of bentonites to release anticorrosion pigments for use on zinc, iron and aluminium has been investigated previously using trivalent rare earth and alkaline earth metals as the exchangeable cations [37–41]. Anionic exchange pigments such as hydrotalcite ($Mg_6Al_2(OH)_{16}CO_3{\cdot}4H_2O$) and hydrotalcite (HT)-like compounds have shown to successfully inhibit filiform corrosion on aluminium [38,42]. HT-like pigments containing phosphate ions have been shown to reduce cathodic delamination of epoxy coatings on steel substrates by forming a insoluble film at the anode [43]. Herein, the influence of Zn^{2+} and PO_4^{3-} ions on cathodic disbondment is investigated separately by using a bentonite cation-exchange pigments system to store and release Zn^{2+}, and a HT anion-exchange pigment as a means of delivering in-coating phosphate ions.

The scanning Kelvin probe (SKP) technique has been used to study cathodic delamination on numerous occasions, and has the ability to measure the potential distributions beneath intact organic coatings [44–48] and obtain mechanistic information pertaining to the use of corrosion inhibitors dispersed in model coatings [9,28,30,35,37,39,40]. In the work to be described here, an in-situ SKP technique is used to monitor the rate at which a coating of polyvinyl butyral co-acetate co-alcohol (PVB) containing dispersed corrosion inhibitor pigments cathodically delaminates from HDG steel. Corrosion inhibitor pigments, based on phosphate exchanged hydrotalcite (HT-Phos), zinc exchanged bentonite (Zn-Ben) and zinc phosphate (ZnPhos) are dispersed, at a 0.02–0.2 pigment volume fraction (ϕ) range, within the model PVB coating. Cathodic disbondment is initiated from an artificial defect created in a Stratmann [45,49] type cell on HDG substrates using aerated sodium chloride ($NaCl_{(aq)}$). The inhibitive efficiency of each pigment type is then compared with the aim of determining the relative contribution of zinc cations (Zn^{2+}) and phosphate anions (PO_4^{3-}) to the inhibition of cathodic delamination afforded by ZnPhos. In so doing we hope to identify the means to improve the efficiency of phosphate-based inhibitive pigment technology in protecting against organic coating failure via a cathodic disbondment mechanism.

2. Experimental details

2.1. Materials

Hot dipped galvanised steel (HDG) was supplied by TATA Steel UK and consisted of 0.7 mm thick, mild steel coated with a 20 μm zinc layer (containing 0.15 wt% aluminium) on each side. 5 cm × 5 cm samples were cut from a larger sheet. Zinc phosphate PZ20 (> 97% purity, ~ 4.5 μm diameter), was supplied by Société Nouvelle des Couleurs Zincique (SNCZ). Sodium-exchanged Wyoming bentonite (grade GG) was obtained from Steetley Bentonites and Absorbents. Polyvinyl butyral-co-vinyl alcohol-co-vinyl acetate (PVB), molecular weight 70,000–100,000, zinc chloride ($ZnCl_2$), hydrotalcite powder (nominal composition: $Mg_6Al_2[OH]_{16}CO_3{\cdot}4H_2O$), and all other chemicals, were obtained from Sigma-Aldrich Chemical Company and of analytical grade purity.

2.2. Methods

2.2.1. Pigment preparation

The methodology used here to prepare HT for use as an anion-exchange pigment has been described in detail previously elsewhere [37,38]. A schematic diagram showing the preparation of phosphate exchange HT is given in Fig. 1. In brief, HT was calcined in air at 450 °C for 3 h to remove CO_2 and water. The remaining MgO-Al_2O_3 (magnesium oxide – alumina) and was left to cool to room temperature. The MgO-Al_2O_3 was then dispersed in 0.5 mol.dm^{-3} aqueous solution of sodium phosphate (Na_3PO_4) which was stirred continuously for 3 h. The resulting HT – PO_4^{3-} anion exchanged pigment was washed by repeated cycles of centrifugation and dispersion in fresh di-stilled water until Na^+ ions were no longer detected using flame emission. Once washed, the pigment was dried in air before undergoing a ball milling process to produce a powder. Henceforth the phosphate exchanged hydrotalcite will be referred to as Phos-HT.

The methodology used to prepare the Zn^{2+} exchanged bentonite pigment has been described in detail elsewhere [27,37,40,50]. In brief, sodium-containing Wyoming bentonite clay powder was dispersed in 1 mol dm^{-3} aqueous solutions of $ZnCl_2$ followed by stirring for 2 h. The suspension was left to settle overnight, and the supernatant was then decanted. The pigment was washed exhaustively by repeated cycles of centrifugation and re-dispersion in fresh di-stilled water, until no Cl^- was detected when the powder was subjected to silver nitrate solution testing. The pigment was dried in air before being ball-milled into a powder. Henceforth zinc exchanged bentonite will be referred to as Zn-Ben.

2.2.2. Coating formulation

In the current work a model coating consisting of PVB was chosen. Although PVB is not fully representative of an industrial coating it offers a suitable alternative whereby its use is for the principal aim of measuring the comparative effect of dispersed pigments on inhibiting cathodic disbondment. PVB coatings are simple to produce and, when unpigmented, will fail relatively rapidly from a range of metallic substrates via cathodic disbondment [9,39]. Therefore, any subsequent changes in coating corrosion performance can be attributed to the dispersion of added pigments. Unpigmented model PVB coatings were formulated by mixing PVB powder in ethanol at 15.5% w/w using a high shear mixer (IKA Ministar 20) at 400 rpm until the powder is fully dissolved. Pigmented PVB coatings were formulated by dispersing the relevant pigment into the PVB model coating at various volume fractions (ϕ). The mass of the pigment (M_{pig}) required for each value of ϕ was determined using Eq. (2), where M_{pol} is the mass of the polymer (0.8 g.cm^{-3}), ρ_{pig} is the density of the relevant pigment and ρ_{pol} is the density of the polymer (1.083 g.cm^{-3}).

$$M_{pig} = \frac{\varnothing \times M_{pol} \times \rho_{pig}}{(1 - \varnothing) \times \rho_{pol}} \quad (2)$$

A thick ethanolic slurry of the pigment is made, before being dispersed at the relevant amount, determined by Eq. (2), into a 15.5% w/w PVB/Ethanol solution using the high shear mixer. The pigmented PVB solution was also degassed using an ultrasonic bath prior to coating application.

2.2.3. Cathodic delamination sample preparation

HDG sheets were cut into 5 cm × 5 cm coupons and the surface oxide on the coupons was removed by polishing using an aqueous slurry of 5 μm alumina powder before degreasing with acetone. A "Stratmann" type corrosion cell was used to create a defect in a model coating of PVB

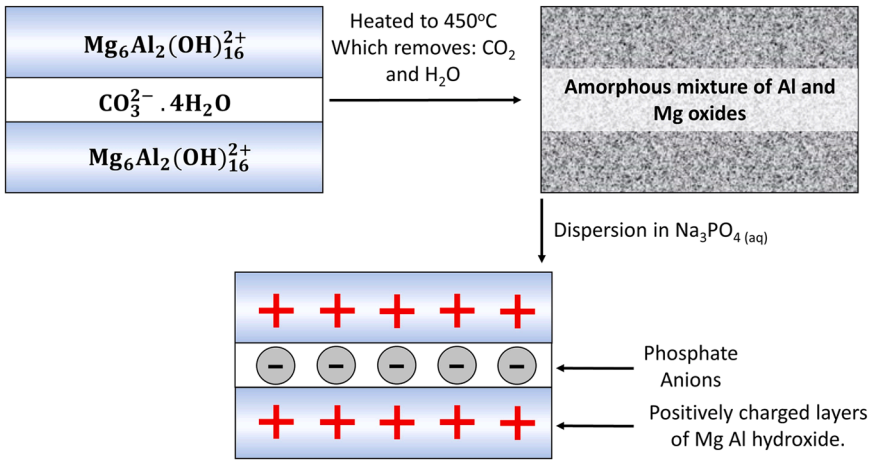

Fig. 1. A schematic showing the process to produce phosphate exchanged hydrotalcite (Phos-HT).

applied to HDG steel by which cathodic disbondment can be initiated [44–46,48]. Electrical insulation tape was applied to parallel edges of each coupon and a piece of 3 M Scotch™ tape was applied to the top edge of the sample. PVB was bar cast onto the bare HDG surface using a glass rod. The PVB coating was left to air dry and the final dry film thickness, as measured using a micrometre gauge, was 30 ± 5 μm. Once the PVB was dry, the scotch tape was carefully pulled up and cut away, revealing a bare HDG section with residual lip of the scotch tape acting as an artificial defect to the intact coating. Non-corrosive silicone rubber was applied to the remaining edges of the defect; forming a reservoir from which cathodic delamination could be initiated by application of a 2 cm^3 volume of 0.86 mol dm^{-3} NaCl (aq), adjusted to pH 7.

2.2.4. Scanning Kelvin probe (SKP)

The SKP apparatus used for this body of work consisted of a 125 μm diameter gold wire reference probe which was vibrated sinusoidally at a frequency of 280-Hz and amplitude of 40 μm. The design and operation of the SKP instrumentation used for potentiometric measurements under atmospheric conditions is described in detail elsewhere [9,44]. The SKP was calibrated in terms of electrode potential using couples of Ag/Ag^+, Cu/Cu^{2+}, Fe/Fe^{2+} and Zn/Zn^{2+}. In brief, metal discs (15 mm diameter, 5 mm thick) were machined to create 8 mm diameter and 5 mm deep wells. These wells were filled with 0.5 mol dm^{-3} aqueous solution of the respective of the metal chloride salt. The SKP probe is vibrated in the centre of the well, 100 μm above the solution meniscus, with the electrode potential of the metal being continuously measured vs. SCE using a Solartron 1280B potentiostat. Following this calibration procedure, the Volta potential difference between the SKP gold reference probe and the polymer/air interface ($\Delta\Psi_{Pol}^{Ref}$) was obtained and used in Eq. (3) to determine the calibration constant (C). Once C has been obtained, Eq. (3) is used to obtain E_{corr} values from the Volta potentials measured by the SKP apparatus.

$$E_{corr} = \Delta\Psi_{Pol}^{Ref} + C\ (V\ vs.\ SHE) \quad (3)$$

Calibration was repeated before and after each SKP experiment. The SKP reference probe along a 12 mm line normal and adjacent to the defect/intact coating boundary, taking 20 E_{corr} data points per mm. Data points were recorded as numerical grids on the control computer. Scans were taken every hour for 24 h unless stated otherwise and were repeated 4 times for each sample. The samples were sealed within a steel chamber, which acted as a Faraday cage. A fixed chamber humidity of 95% was achieved by using petri dish reservoirs of 0.86 mol dm^{-3} $NaCl_{(aq)}$ on the chamber floor and the temperature was maintained at a constant 20 °C.

3. Results and discussion

3.1. Delamination of unpigmented coatings

To enable a systematic study into the effect of varying ϕ on the kinetics and mechanism of cathodic disbondment, baseline kinetics were initially established in the absence of pigment. Baseline kinetics were produced by measuring the rate of cathodic delamination of an unpigmented PVB coated HDG steel sample once initiated with 0.86 mol dm^{-3} $NaCl_{(aq)}$. Once the corrosion-driven cathodic coating failure becomes established, SKP-derived, time-dependent E_{corr} vs. distance (x) profiles, typified in Fig. 2(a) can be obtained and correlated with various regions of the underfilm corrosion cell. The $E_{corr}(x)$ profile can be divided in four distinct regions, as follows:

Region (1) (labelled on Fig. 2(a)) is associated with the coated substrate immediately adjacent to the defect area where corrosive $NaCl_{(aq)}$ is in contact with exposed Zn and is undergoing anodic metal dissolution according to reaction (4). A corresponding drop in E_{corr} value, close to

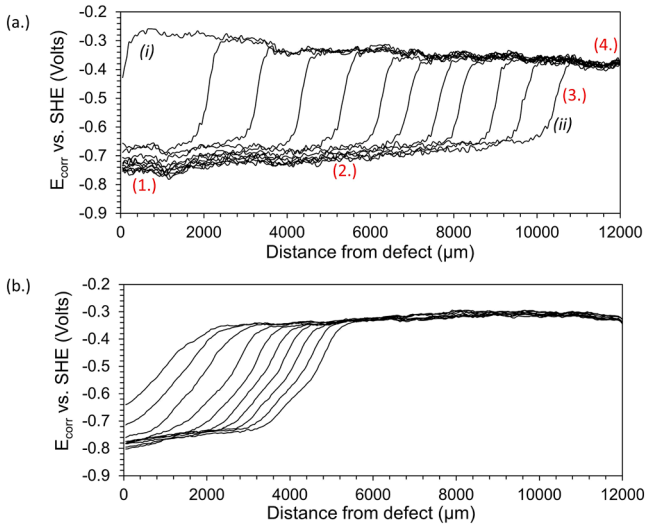

Fig. 2. An E_{corr} vs. distance from defect (x_{del}) profile recorded using the SKP technique to measure the time dependent delamination of an unpigmented PVB coated HDG substrate initiated with (a) 0.86 mol dm^{-3} $NaCl_{(aq)}$ and (b) 0.01 mol dm^{-3} sodium phosphate (Na_3PO_4) added to 0.86 mol dm^{-3} $NaCl_{(aq)}$. Time key: (a) curve *(i)* = 60 min with every curve after recorded 120 min thereafter until the end of the experiment at *(ii)*. (b) curve *(i)* = 240 min with every curve after recorded 120 min thereafter until the end of the experiment at *(ii)*.

that of freely corroding zinc (ca. −0.75 V vs. SHE) is recorded by the SKP [9,44].

$$Zn_{(s)} \leftrightharpoons Zn^{2+}_{(aq)} + 2e^- \quad (4)$$

$$O_2 + 2H_2O + 4e^- \leftrightharpoons 4OH^-_{(aq)} \quad (5)$$

Region (2) represents the delaminated area of coating where ionic migration occurs in the underfilm electrolyte. The potential change across the length of this delaminated zone is due to the passage of ionic current within a thin electrolyte layer of significantly higher resistivity than the original initiating electrolyte applied to the defect. Region (3) is the cathodic front where disbondment occurs and is shown in the $E_{corr}(x)$ plot as a sharp gradient linking the principal underfilm cathode with the delaminated region behind. Region (4) comprises the intact (uncorroded) area to the right of the delamination front, where the PVB remains adhered to the underlying Zn (ca. −0.32 V vs. SHE)) [9]. The sharp gradient in E_{corr} associated with the delamination front is a convenient way to identify the delamination distance (x_{del}) which can be used in conjunction with holding time as a means of quantifying cathodic disbondment kinetics. Disbondment occurs at Region (3) due to the cathodic oxygen reduction reaction (ORR) producing an alkaline environment (pH ≥10) via reaction (5). This will cause the dissolution of surface zinc (hydr)oxide to soluble zincate (reaction (6) and (7)). The zinc surface may directly oxidise at pH > 10.37 (reaction (8)). The increased pH has also been reported to cause base catalysed hydrolysis of vinyl acetate functions within the PVB which contribute to coating disbondment [9,44,45].

$$Zn(OH)_2 \leftrightharpoons HZnO^-_{2(aq)} + H^+_{(aq)} \quad (6)$$

$$Zn(OH)_2 \leftrightharpoons ZnO^{2-}_{2\ (aq)} + 2H^+_{(aq)} \quad (7)$$

$$Zn_{(s)} + 2H_2O \leftrightharpoons HZnO^-_{2(aq)} + 3H^+_{(aq)} + 2e^- \quad (8)$$

Phosphate has been shown to behave as a mixed inhibitor of zinc, steel and iron corrosion [1,51,52] and is therefore likely to affect both the anodic and cathodic reactions. Applying a phosphate-based electrolyte directly to the defect electrolyte will determine whether phosphate influences the kinetics of coating failure by suppressing the net anodic reaction occurring on the exposed Zn metal. To this end, 0.01 mol dm^{-3} sodium phosphate (Na_3PO_4) was dissolved in 0.86 mol dm^{-3} $NaCl_{(aq)}$, adjusted to pH 7 and applied to the defect to initiate cathodic disbondment of an unpigmented PVB coated HDG sample. Fig. 2(b) shows a plot of E_{corr} as a function of delamination distance (x_{del}) recorded after initiation. The initiation period preceding the onset of corrosion-driven cathodic disbondment has been reported in previous work [9,44,45] and is due to the time required for electrolyte to penetrate under the PVB coating to support electrochemical activity. The delamination front progressed a maximum of 4.6 mm away from the defect after 24 h, which when compared to equivalent data for the un-inhibited case given in Fig. 2(a) showing a 10.5 mm disbondment distance after the same holding time, represents a reduction of 56%. Visual inspection of the defect regions of both specimens after 24 h showed an appreciable accumulation of white corrosion product on the exposed metal in the absence of inhibitor, but very little in the presence of a 0.01 mol dm^{-3} concentration of dissolved phosphate. Therefore, although there is evidence that dissolved phosphate strongly inhibits zinc dissolution in the defect region by precipitating a film of zinc phosphate ($Zn_3(PO_4)_2$) over anode sites [24], this is insufficient to halt the propagation of cathodic delamination of the adjacent PVB. Consequently, the extent of cathodic delamination is only slowed by the presence of phosphate compared to the uninhibited case. In addition, given the solubility of zinc phosphate (($Zn_3(PO_4)_2$ $K_{sp} = 9 \times 10^{-33}$ mol^3dm^{-9}), the saturated concentration of phosphate ions which could accumulate in the defect electrolyte as a result of leaching from in-coating $Zn_3(PO_4)_2$ is 3.06×10^{-7} mol dm^{-3} which is significantly lower than the 0.01 mol dm^{-3} level used here. Fig. 3 shows a plot of x_{del} vs. $(t_{del} - t_i)^{1/2}$ obtained from the various E_{corr} (x) curves shown in Fig. 2 (b), where t_{del} is the time from corrosion initiation and t_i is the time taken for the delamination cell to become established. The plots show a straight line for electrolytes both in the presence and absence of sodium phosphate, indicating that the rate of coating failure remains controlled by ionic mass-transport in the underfilm electrolyte, even in the presence of inhibitor. As such, it appears that phosphate inhibition at the defect never becomes sufficiently complete and that coating delamination rate is controlled by reaction (4) within the underfilm delaminated region. Rate of coating disbondment can be determined by the slope of the lines presented in Fig. 3 whereby the uninhibited coating has a slope of 406 μm $min^{1/2}$ reduced to 236 μm $min^{1/2}$ when phosphate is present in the external electrolyte. A similar result was observed by Williams et al. when investigating the inhibition of corrosion driven cathodic disbondment of PVB coatings containing strontium chromate [9]. Williams et al. reported that chromate was unable to inhibit cathodic delamination when available in the defect electrolyte but was far more effective when used within a coating where it completely inhibited underfilm corrosion-driven failure. In a similar manner, the findings reported here clearly indicate that phosphate ions leaching from a coating into an external electrolyte are unlikely to substantially affect rates of corrosion-driven coating disbondment.

3.2. Delamination of ZnPhos pigmented coatings

Prior to investigating the influence of phosphate and Zn^{2+} separately a benchmarking investigation was carried using industry standard ZnPhos pigment. ZnPhos was dispersed in model PVB coating at a range of different pigment volume fractions (ϕ) in order to study the effect on cathodic delamination rate when compared with an unpigmented PVB coating. Plots of time dependent $E_{corr}(x)$ profiles are shown in Fig. 4 for coatings containing (a.) 0.05 ϕ and (b.) 0.2 ϕ ZnPhos. Table 1 shows information such as t_i and E_{intact} which are obtained from Fig. 4.

Coating disbondment kinetics can be obtained by studying Fig. 5 which shows the delamination distance (x_{del}) as a function of time $(t_{del}-t_i)^{1/2}$ for all value of ZnPhos ϕ. The curves in Fig. 5 show that kinetics remain parabolic at all ZnPhos ϕ. The retention of parabolic kinetics has been observed previously for pigmented PVB coatings containing group II and rare-earth metal loaded bentonites [28,39]. In these studies, it was stated that the rate limiting step is the migration of Na^+ ions in the underfilm electrolyte which is also the case in terms of ZnPhos. However, this observation is at odds with other investigations of in-coating Zn^{2+} studies on zinc surfaces where linear kinetics were observed [27]. The difference in kinetics is almost certainly due to the higher availability of Zn^{2+} in the previous work compared to the limited

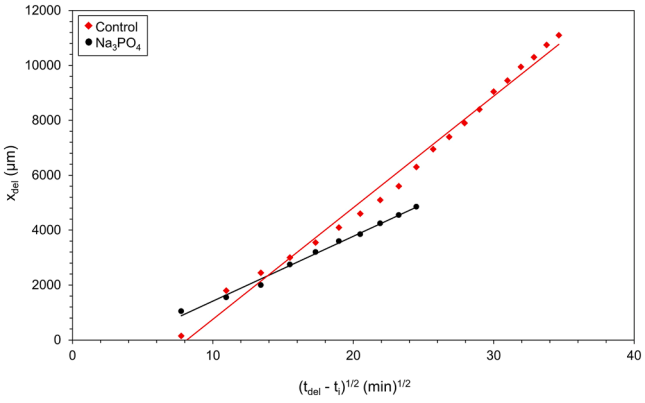

Fig. 3. Plots of delamination distance (x_{del}) as a function of delamination time $(t_{del}-t_i)^{1/2}$ for unpigmented PVB coatings on HDG substrate. Electrolyte used to initiate corrosion is (a) 0.86 mol dm^{-3} $NaCl_{(aq)}$ and (b) 0.01 mol dm^{-3} sodium phosphate (Na_3PO_4) added to 0.86 mol dm^{-3} $NaCl_{(aq)}$.

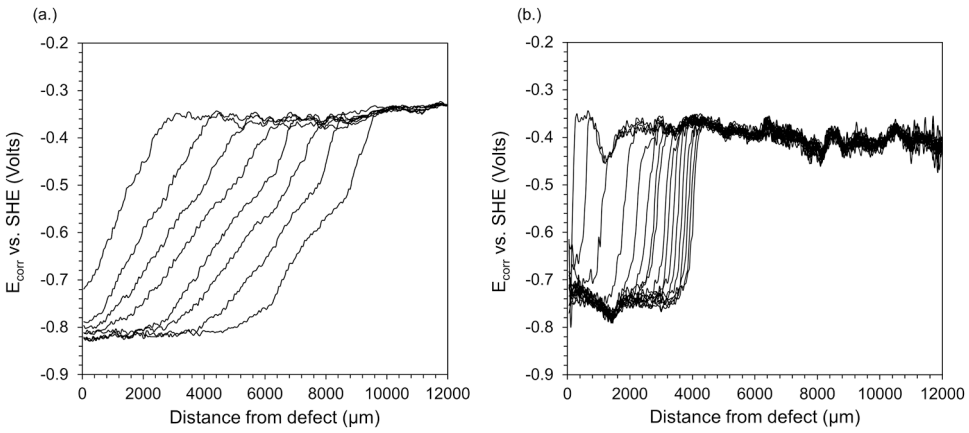

Fig. 4. Profiles of E_{corr} vs. distance from defect (x_{del}) recorded using the SKP technique to measure the time dependent delamination of a PVB coated HDG substrate pigmented with a.) 0.05 ϕ ZnPhos, b.) 0.2 ϕ ZnPhos.

Table 1
Values of the cathodic delamination rate constant (k_{del}), inhibition efficiency, delamination initiation time (t_i) and intact potential (E_{intact}) obtained for the delamination of PVB, containing varying ϕ of Phos-HT, ZnPhos and Zn-Ben from a HDG substrate.

Pigment (ϕ)	k_{del} (μm $min^{-1/2}$)	k_{del} reduction (%)	t_i (min)	E_{intact} vs. SHE (V)
Control	406	–	0	-0.32 ± 0.02
ZnPhos 0.05	267	20	60	-0.35 ± 0.03
ZnPhos 0.1	143	66	450	-0.37 ± 0.04
ZnPhos 0.2	149	65	180	-0.39 ± 0.04
Phos-HT 0.02	284	27	240	-0.33 ± 0.03
Phos-HT 0.05	160	55	540	-0.48 ± 0.01
Phos-HT 0.1	99	75	240	-0.49 ± 0.02
Phos-HT 0.2	93	78	1020	-0.48 ± 0.02
Zn-Ben 0.02	4.57 (μm min^{-1})	58	840	-0.48 ± 0.02
Zn-Ben 0.05	1.81 (μm min^{-1})	84	1920	-0.55 ± 0.03
Zn-Ben 0.1	0	100	–	-0.57 ± 0.02

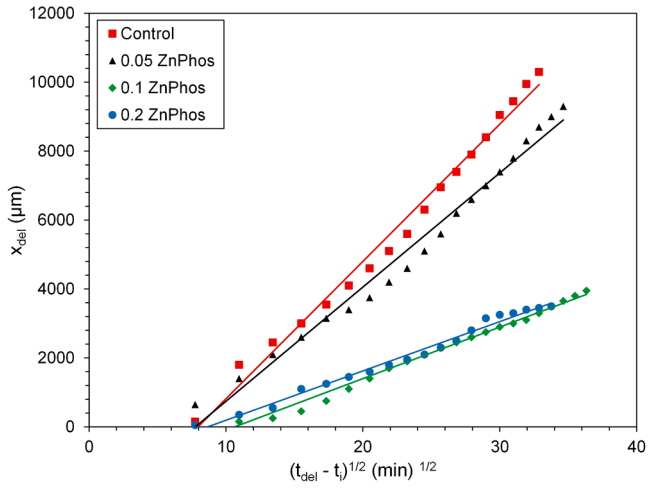

Fig. 5. Plots of delamination distance (x_{del}) as a function of delamination time $(t_{del}\text{-}t_i)^{1/2}$ for unpigmented and ZnPhos pigmented PVB coated HDG substrate, derived from SKP E_{corr} vs. x_{del} profiles for each ZnPhos ϕ.

availability of Zn^{2+} provided by ZnPhos due to the low solubility of the pigment. ZnPhos is found to have limited effect at inhibiting corrosion driven cathodic disbondment on HDG steel but was able to slow the rate by a maximum of 66% at 0.1 ϕ compared to an unpigmented control. Parabolic rate constants (k_{del}) obtained from Fig. 5 are reported in Table 1.

3.3. Delamination of Phos-HT pigmented coatings

The effect of Phos-HT pigments on the rate of cathodic disbondment was investigated by systematically changing the amount of pigment dispersed within the PVB coating from 0.02 to 0.2 ϕ. Fig. 6 shows the time dependent E_{corr} vs. distance (x_{del}) profiles obtained for Phos-HT: (a.) 0.02 ϕ (b.) 0.05 ϕ (c.) 0.1 ϕ and (d.) 0.2 ϕ. Table 1 gives values for initiation time (t_i) and intact coating potential (E_{intact}) obtained from Fig. 6. The initiation time (t_i) is the time at which a cathodic delamination front, characterised by a sharp drop in E_{corr} is first detected towards the left-hand side of the scanned area of the PVB coated zinc surface. There is evidence that increasing additions of Phos-HT delays the onset of cathodic disbondment as t_i increases from 240 min at 0.02 ϕ to 1020 min for 0.2 ϕ. The potential values recorded at the intact coating (E_{intact}) are suppressed for all Phos-HT ϕ compared to the control. The value of E_{intact} can be interpreted in terms of the underfilm reduction of atmospheric O_2 on the passive (uncorroded) Zn surface as well as Brønsted-lowry acid-base reactions that occur between the metal surface and the organic coating [46,53]. Values of E_{intact} are suppressed to ~ − 0.49 V vs. SHE for coatings containing 0.1ϕ Phos-HT compared to ~ − 0.32 V vs. SHE for the control (unpigmented coating). A suppression of E_{intact} is consistent with the Phos-HT providing a net cathodic inhibition, based on mixed potential theory. A similar effect of cathodic suppression of the intact coating potential was reported by Klimow et al. during their work on phosphate conversion coated zinc [54]. However, we cannot rule out non-Faradic contributions to the supressed E_{intact} measurements. This effect occurs due to the phosphate anions present in the coating which can adsorb onto the zinc (hydr)oxide surface [9]. The net negative charge of the adsorbed phosphate ions could act to suppress the potential at the coating-metal interface.

Rates of coating disbondment are given in Fig. 7, in which x_{del} is plotted as a function of the square root of delamination time $(t_{del}\text{-}t_i)^{1/2}$ for all Phos-HT ϕ. Values of k_{del} for each Phos-HT ϕ are given in Table 1 along with percentage reduction in rate compared to an unpigmented coating. The plots given in Fig. 7 show that all x_{del} vs. $t^{1/2}$ plots are linear, indicating the predominance of parabolic kinetics. The retention of parabolic kinetics is associated with the rate of coating delamination remaining controlled by the migration of cations (Na^+) and ion conductivity in the underfilm electrolyte [9] even in the presence of

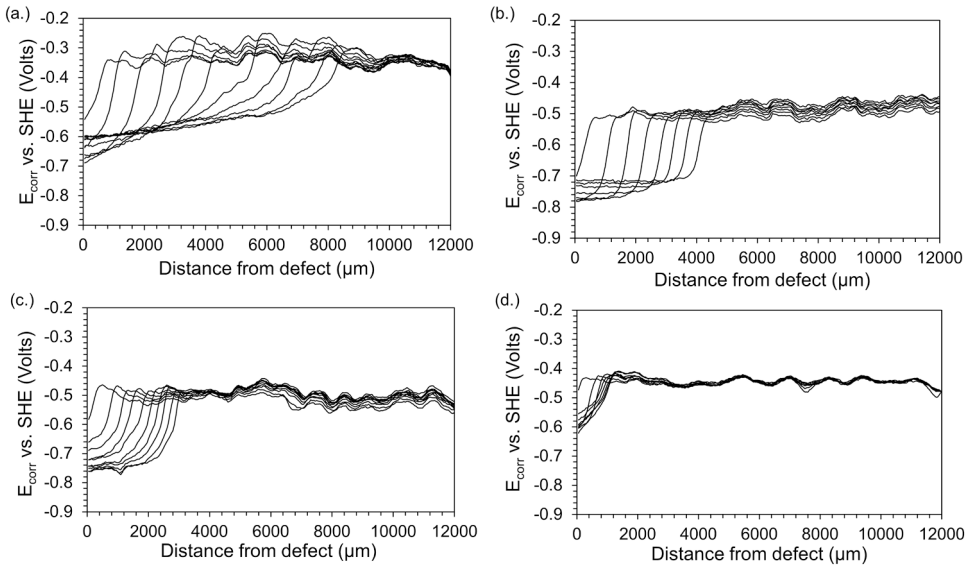

Fig. 6. Profiles of E_{corr} vs. distance from defect (x_{del}) recorded using the SKP technique to measure the time dependent delamination of a PVB coated HDG substrate pigmented containing (a.) 0.02 ϕ Phos-HT, (b.) 0.05 ϕ Phos-HT,(c.) 0.1 ϕ Phos-HT, (d.) 0.2 ϕ Phos-HT once corrosion is initiated using 0.86 M NaCl.

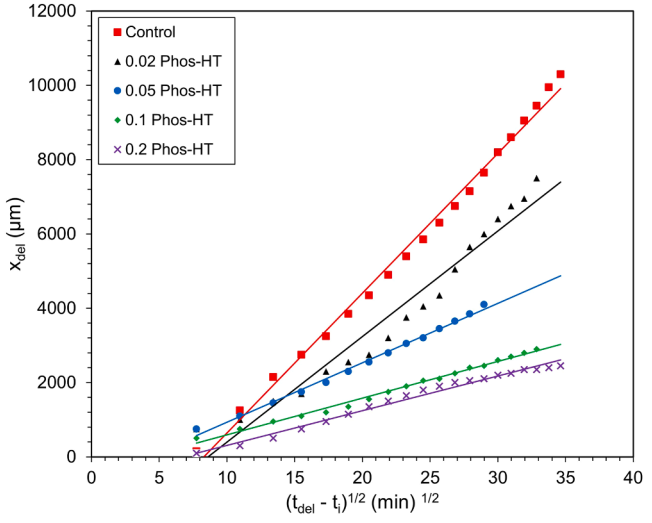

Fig. 7. Plots of delamination distance (x_{del}) as a function of delamination time $(t_{del}\text{-}t_i)^{1/2}$ for unpigmented and Phos-HT pigmented PVB coated HDG substrate, derived from SKP E_{corr} vs. x_{del} profiles for each Phos-HT ϕ.

in-coating Phos-HT inhibitive pigment. Parabolic kinetics can also occur through degradation during cathodic disbondment which arises due to pH dependent coating porosity, however it is likely that rate limitation by ionic mass transport remains the most likely cause [55,56]. Table 1 shows that delamination rate progressively decreases with increasing Phos-HT ϕ. However, even at the highest ϕ of 0.2, Phos-HT is unable to stop cathodic disbondment and a maximum reduction of 78% in k_{del} is measured in comparison to an unpigmented sample.

The parabolic kinetics associated with the delamination of pigmented PVB from HDG have been reported in previous work using in-coating smart-release inhibitive pigments loaded with cerium (III) cations [40] and calcium (II) cations [28]. The retention of parabolic kinetics whilst producing a significant decrease in the rate of delamination can be explained be two theories. The first is that the mass transport of cations in the underfilm electrolyte has become more tortuous with increasing Phos-HT ϕ. The form of phosphate released from Phos-HT pigment is pH dependent shown in the dissociation of phosphoric acid given in reactions (9)–(11).

$$H_3PO_4 \leftrightharpoons H_2PO_4^- + H^+ \; [pK_{a1} = 2.14] \tag{9}$$

$$H_2PO_4^- \leftrightharpoons HPO_4^{2-} + H^+ \; [pK_{a2} = 7.2] \tag{10}$$

$$HPO_4^{2-} \leftrightharpoons PO_4^{3-} + H^+ \; [pK_{a2} = 12.4] \tag{11}$$

The alkaline environment that forms at the cathodic front due to ORR has been reported to reach a pH > 10 [44] and so phosphate would be released into the underfilm electrolyte as hydrogen phosphate HPO_4^{2-} via reaction (10). The increase in tortuosity of cation transport in the underfilm electrolyte could be provided by the formation of a precipitate. This may occur due to small concentrations of Zn^{2+} present in the underfilm electrolyte reacting with exchanged phosphate anions to form zinc phosphate via reaction (12).

$$2HPO_4^{2-} + 2OH^- + 3Zn^{2+} \leftrightharpoons Zn_3(PO_4)_2 + 2H_2O \tag{12}$$

However, there is likely to be a very low concentration of Zn^{2+} at the cathodic site due to the alkaline pH which would allow zincate to form via reactions (6)–(8). Further to this, Tomandl et al. suggests that solid state phosphate will remove hydroxide from electrolyte to form $Zn(OH)_2$ directly rather than the mechanism stated in reaction (12) [57]. The second, and more likely, possibility is that the mobility of under-film electrolyte ionic transport is unaffected, but the charge required to be passed per unit of disbondment has increased. The increase in under-film ohmic resistance can occur due to buffering of electrolyte pH. Phosphate can act as a pH buffer if it is available in the under-film electrolyte deprotonated form of hydrogen phosphate (HPO_4^{2-}) by absorbing hydroxide formed at the ORR via reaction (13).

$$H_2PO_4^- + OH^- \rightarrow HPO_4^{2-} + H_2O \tag{13}$$

Ogle et al. has suggested this mechanism of inhibition is afforded by phosphate in the use of phosphate pre-treatments on zinc subjected to alkaline conditions [58]. Allahar et al. and Huang et al. have shown through the development of mathematical models that the coating porosity and polarization kinetics can be treated as a function of pH [55, 56]. The buffering of pH through reaction (13) would reduce the pH dependent bond breaking reactions that cause increased coating porosity. This would correspond in the reduction in rate of cathodic disbondment observed.

Both modes of in-coating phosphate inhibition discussed here would necessarily increase the resistivity of the underfilm electrolyte in the

delaminated zone. Therefore, it is anticipated that the E_{corr} versus distance (x) profiles for Phos-HT pigmented PVB coatings should confirm this by producing a greater iR drop in the region linking the cathodic disbondment front with the coating-defect boundary, when compared with the unpigmented case. Indeed a delaminated zone dE/dx slope of 4 mV/mm determined for an unpigmented PVB coating after a 24 h holding time (see Fig. 2a) increased to ca 12 mV/mm when Phos-HT pigment at $\phi = 0.02$ and 0.1 was dispersed within the coating (see Fig. 6a and c). In the case of a higher pigment loading of $\phi = 0.2$ (Fig. 6d), the E_{corr}-x profile after 24 h has not developed significantly to differentiate between the disbondment front and the delaminated zone. The one inconsistency seems to be the data in Fig. 6(b) where the delaminated zone slope seems to tend to zero as a result of apparent passivation in the underfilm region immediately adjacent to the defect, which does not seem to be representative of general behaviour for the other pigmented coatings. Despite this one exception, it seems that in general Phos-HT pigmented coatings demonstrate a higher iR drop than unpigmented PVB in the delaminated zone and as such provides support for an inhibition mechanism which generates increased resistivity of the underfilm electrolyte.

3.4. Delamination of Zn-Ben pigmented coatings

The effect to Zn-Ben pigments on the rate of cathodic disbondment was investigated by systematically changing the amount of pigment dispersed within the PVB coating from 0.02 to 0.1 ϕ. Fig. 8 shows the time dependent E_{corr} vs. distance (x_{del}) profile for a PVB coating containing 0.05 ϕ Zn-Ben. The holding time was increased from 24 to 48 h for this experiment due to the delay in the onset of corrosion. No delamination was recorded after 24 h and a maximum delamination of 1.5 mm was recorded after 48 h. The E_{intact} value recorded for 0.05 ϕ Zn-Ben (-0.55 ± 0.03 V) which is significantly suppressed compared to an unpigmented coating (-0.32 ± 0.02 V). This suppression is consistent with net cathodic inhibition. Further evidence of cathodic inhibition can be obtained by studying Fig. 9 which shows the kinetics of coating delamination in the presence of Zn-Ben ϕ. Fig. 9 shows plots of x_{del} versus t_{del} for $0.02 \leq \phi < 0.1$ Zn-Ben and it is observed that rate of cathodic disbondment decreases with increasing ϕ and tend to zero for $\phi \geq 0.1$. It is also evident that for all ϕ Zn-Ben that there is a change in kinetics from parabolic to linear. This change in kinetics implies that underfilm suppression of the cathodic reduction reaction, rather than ionic mass transport rates, is primarily responsible for the inhibition provided by coatings containing Zn-Ben pigments. Table 1 gives values of $t_{(i)}$ and E_{intact} that are obtained from Fig. 8 and k_{del} from Fig. 9.

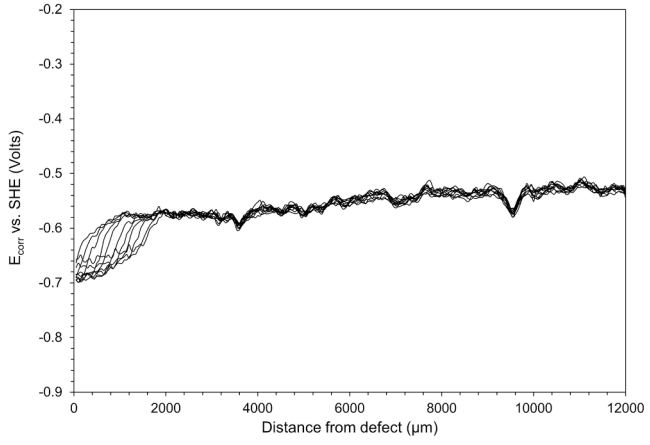

Fig. 8. Profiles of E_{corr} vs. distance from defect (x_{del}) recorded using the SKP technique to measure the time dependent delamination of a PVB coated HDG substrate pigmented with 0.05 ϕ Zn-Ben.

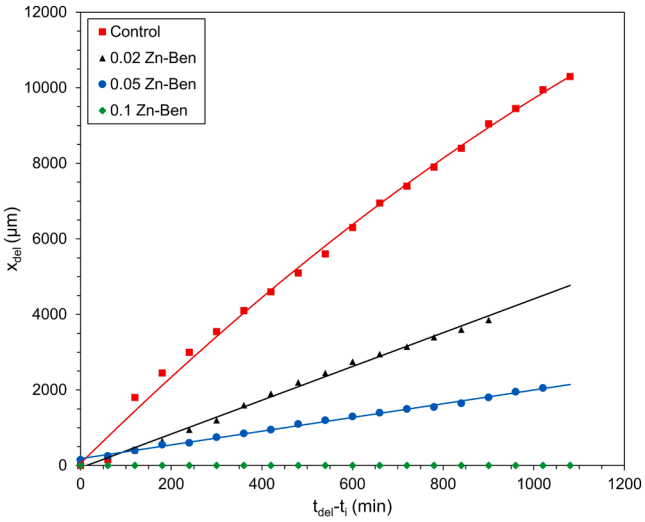

Fig. 9. Plots of delamination distance (x_{del}) as a function of delamination time $(t_{del}\text{-}t_i)^{1/2}$ for unpigmented and Zn-Ben pigmented PVB coated HDG substrate, derived from SKP E_{corr} vs. x_{del} profiles for each Zn-Ben ϕ.

4. Discussion

PVB coatings containing ZnPhos were only able to inhibit corrosion driven coating disbondment on HDG steel by a limited extent, with the greatest inhibition provided at 0.1 ϕ, which reduced the rate by 66% compared to an unpigmented coating. Parabolic kinetics were observed for all ZnPhos ϕ which indicates that the rate limiting step remains under-film ionic mass transport. It was suggested by Wint et al. that ZnPhos may reduce the rate of cathodic disbondment by buffering the underfilm electrolyte pH via reaction (14) and (15). Buffering the pH will reduce the rate of zinc hydr(oxide) dissolution and base catalyzed hydrolysis of vinyl acetate functions within the PVB coating which contribute to coating disbondment [25].

$$Zn^{2+} + 4OH^- \leftrightharpoons Zn(OH)_4^{2-} \quad (14)$$

$$Zn_3(PO_4)_2 + 12OH^- \leftrightharpoons 3Zn(OH)_4^{2-} + 2PO_4^{3-} \quad (15)$$

The use of ZnPhos as a corrosion inhibitor pigment has been studied extensively elsewhere [15,19,24,51,59–62] and its limited performance has been suggested to be due to the its low solubility ($K_{sp} = 9 \times 10^{-33}$ mol^3dm^{-9}). Using the K_{sp} of zinc phosphate, the equilibrium concentration of Zn^{2+} and phosphate ions released into the underfilm electrolyte is calculated to be 4.6×10^{-7} mol dm^{-3} and 3.1×10^{-7} mol dm^{-3} respectively. Group II cations, such as Zn^{2+}, released into the aqueous underfilm electrolyte will form hexaquo-complexes that undergo hydrolysis deprotonation at elevated pH. The hydrolysis coefficient (pK_{a1}) is the pH associated with the formation of the hydroxide precipitate via reaction (16),

$$M^{2+} + 2H_2O \leftrightharpoons M(OH)_2 + 2H^+ \quad (16)$$

where M is a group 2 metal. In the case of Zn^{2+} reaction (16) would form $Zn(OH)_2$ which has K_{sp} of 1.74×10^{-17} mol^{-3} dm^{-9} and a pK_{a1} of 8.96. Assuming that the underfilm electrolyte is 10^{-3} mol dm^{-3} $NaOH_{(aq)}$ (pH 11) [45,63] and using the latter K_{sp} associated with $Zn(OH)_2$, it can be calculated that the concentration of Zn^{2+} required to form solid $Zn(OH)_2$ is 1.74×10^{-11} mol dm^{-3}. The amount of Zn^{2+} released by ZnPhos is substantially more than is required to form $Zn(OH)_2$, however the inhibition observed does not match that of Zn-Ben. The rate at which Zn^{2+} is released into the underfilm electrolyte may limit the inhibition afforded by ZnPhos. Previous work by Williams et al. demonstrated that although a high concentration of Zn^{2+} was able to be released by ion exchange pigments the most profound inhibition was observed from the

ion exchange pigment that was able to release the Zn^{2+} quickest [30]. ZnPhos is a sparingly soluble salt which requires an increase in pH to become more soluble and the time required for this to occur may not be sufficient for an adequate concentration of Zn^{2+} to be released to form $Zn(OH)_2$ before the corrosion front progresses. This indicates that the formation of $Zn(OH)_2$ is unlikely to be the main mechanism of inhibition afforded by ZnPhos and that the buffering of underfilm pH given in reactions (14) and (15) is the more likely cause of inhibition.

Fig. 10 shows the comparison of delamination rates (k_{del}) of cathodic disbondment for PVB coatings containing various ϕ of Phos-HT, ZnPhos and Zn-Ben. It should be noted that because of the difference in coating kinetics observed, where ZnPhos and Phos-HT display parabolic and Zn-Ben display linear kinetics, that different y axis is employed to summarise the results. The graph shows that for all pigmented coatings that increasing the ϕ of pigment within the coating reduces the rate of cathodic disbondment. The graph also shows the relative efficiency of the different inhibitor pigments to reducing the rate of cathodic disbondment, whereby the most to least efficient is Zn-Ben > Phos-HT > ZnPhos. Both ion-exchange based inhibitor pigments exceeded the corrosion inhibition performance provided ZnPhos although they each contain only one of the active ions released by ZnPhos when used as a corrosion inhibitor pigment. The limited solubility of ZnPhos means that low concentrations of its constituent ions are released into the underfilm electrolyte during corrosion driven cathodic disbondment, via reaction (1). Low concentrations of anion capable of pH buffering in the underfilm electrolyte will allow for the increase in OH^- ion concentration due to the oxygen reduction reaction making the removal of local zinc hydr (oxide) layer via reaction (17) more likely. This would not be the case for Zn-Ben or Phos-HT whereby they release Zn^{2+} or PO_4^{3-} in an exchange with ions that are available in the underfilm electrolyte.

$$Zn(OH)_2 + 2(OH)^- \rightarrow Zn(OH)_4^{2-} \quad (17)$$

Studying Fig. 10 it is clear that coatings containing Zn-Ben are superior at inhibiting cathodic disbondment compared to those containing Phos-HT. A reason for this can be deduced by the mechanisms by which the pigments inhibit the cathodic disbondment. Fig. 11 shows a graph comparing the E_{intact} values for all values of ZnPhos, Phos-HT and Zn-Ben ϕ tested. The graph shows that all pigmented samples supress E_{intact} potential compared to an unpigmented coating, however Zn-Ben provides the greatest suppression at any value of ϕ with − 0.57 V vs SHE recorded for 0.1 ϕ. A suppression in E_{intact} is consistent with a net cathodic inhibitor and a more negative measurement for coating containing Zn-Ben indicate a more profound inhibition of underfilm cathodic oxygen reduction via reaction (4) compared to that seen by

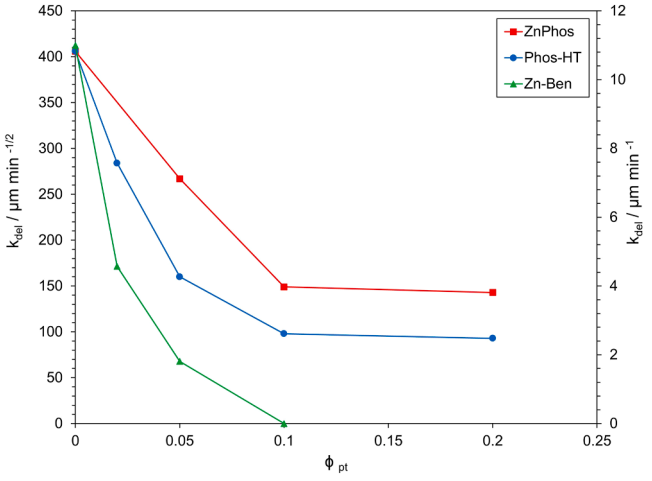

Fig. 10. Comparison of cathodic delamination rate constant (k_{del}) as a function of Phos-HT ϕ, Zn-Phos ϕ and Zn-Ben ϕ.

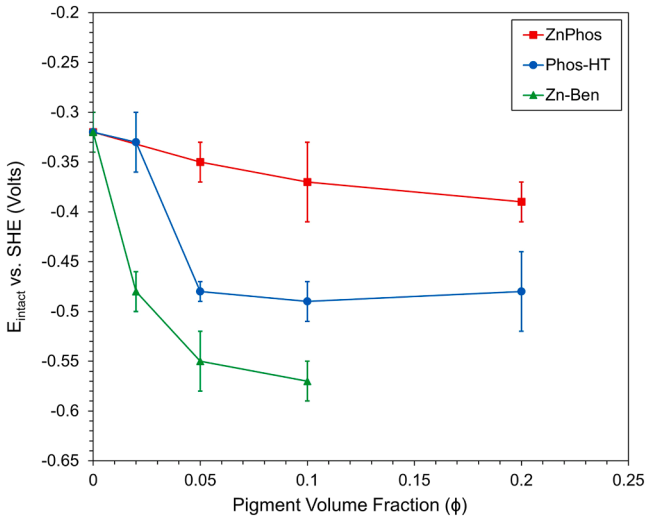

Fig. 11. Summary plots of average E_{intact} as a function of pigment volume fraction (ϕ) for Phos-HT, ZnPhos and Zn-Ben pigments dispersed in PVB coatings. Values of E_{intact} were taken as an average of E_{intact} after 15 h.

coatings containing Phos-HT or Zn-Phos. Further evidence of cathodic inhibition is observed by the change in corrosion kinetics measured for Zn-Ben, which become linear, compared to that of coatings containing Phos-HT or Zn-Phos, which remain parabolic. Williams et al. proposed that Zn^{2+} released by Zn-Ben in the underfilm electrolyte will hydrolyse to precipitate zinc hydr(oxide) ($Zn(OH)_2$) at the cathode, via reaction (16) [28]. This hydrolysis reaction reduces the corrosion rate in two ways. The first is that the reaction removes free OH^- ions from the underfilm electrolyte which acts to buffer pH, preventing the dissolution of amphoteric zinc hydr(oxide) from the surface. The second is that the reaction acts to further thicken this surface zinc hydr(oxide) layer. Zinc hydr(oxide) is a wide band gap ($E_g \sim 3.2$ eV[2]) semi-conductor making it a poor conductor of electricity [16]. Therefore, increasing the thickness of zinc hydr(oxide) provides resistance to interfacial electron transfer which reduces the cathodic oxygen reduction reaction. Coatings containing Zn-Ben ϕ ≥ 0.1 provide high enough concentration of Zn^{2+} at the cathode to stop the reaction from occurring and so completely inhibit cathodic disbondment.

The inhibition afforded by PVB coatings containing Phos-HT was limited to reducing the rate of corrosion driven cathodic disbondment by a maximum of 78% at 0.2 ϕ and corrosion kinetics remained parabolic for all ϕ. It is likely that released phosphate at the cathode will buffer underfilm electrolyte pH by reaction (13) which reduces the rate of zinc hyr(oxide) dissolution and is shown schematically in Fig. 12(c). The inhibition provided by coatings containing Phos-HT is similar to that provided by coatings containing ZnPhos where neither pigment is able to stop cathodic disbondment and corrosion kinetics remain parabolic. Naderi et al. [64] has shown that ZnPhos releases more PO_4^{3-} than Zn^{2+} at elevated pHs therefore it is likely that ZnPhos releases enough PO_4^{3-} into the underfilm electrolyte to slow the rate of cathodic disbondment in the same manner as that observed by coating containing Phos-HT (Fig. 12(b)). However, there is insufficient Zn^{2+} released to promote the formation of zinc hydr(oxide) via Fig. 12(c) and provide the level of inhibition seen by that of Zn-Ben.

5. Conclusions

This paper describes an in-situ investigation using the scanning Kelvin probe to evaluate the inhibition of corrosion-driven cathodic disbondment of PVB coated HDG steel by phosphate exchanged hydrotalcite (Phos-HT) and zinc exchange bentonite (Zn-Ben). Results are compared to determine whether phosphate (PO_4^{3-}) or zinc (Zn^{2+})

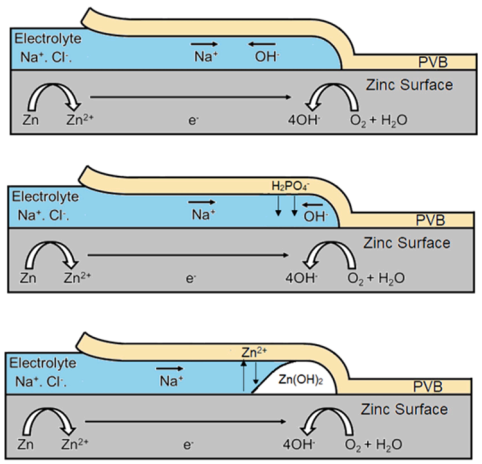

(a.) No inhibitive ions present at the cathode:

$$Zn(OH)_{2(s)} + 2OH^-_{(aq)} \rightarrow Zn(OH)^{2-}_{4\,(aq)}$$

(b.) Coating released $H_2PO_4^-$ available at the cathode:

$$H_2PO_4^-{}_{(aq)} + OH^-_{(aq)} \rightarrow HPO_4^{2-}{}_{(aq)} + H_2O_{(aq)}$$

(c.) Coating released Zn^{2+} available at the cathode:

$$Zn(OH)_{2(s)} + Zn^{2+} + 2OH^-_{(aq)} \rightarrow 2Zn(OH)_{2(s)}$$

Fig. 12. Schematic of the underfilm corrosion mechanisms that occur during the cathodic disbondment of a model coating on HDG steel with the under-film electrolyte containing: (a.) no inhibitive ions, (b.) $H_2PO_4^-$ and (c.) Zn^{2+}.

contribute most heavily to the inhibition afforded by zinc phosphate (ZnPhos) [25,28]. Model coatings of PVB containing 0.02 – 0.2 ϕ Phos-HT were applied to galvanised HDG steel to create "Stratmann" type delamination samples [44–46,48]. It was found that;

- The rate of corrosion driven cathodic disbondment decreased with increasing ϕ of Phos-HT with a maximum reduction of 78% recorded at 0.2 ϕ compared to an unpigmented PVB coating. However, Zn-Ben reduced cathodic disbondment rate to zero at $\phi \geq 0.1$ which shows that coatings containing Zn^{2+} provides greater inhibition to corrosion driven cathodic disbondment of PVB coatings from HDG steel compared to that of coatings containing PO_4^{3-}.
- Corrosion kinetics remained parabolic throughout for PVB coatings containing Phos-HT ϕ which has also been observed in the case of disbondment of PVB coatings containing ZnPhos. ZnPhos provided similar inhibition to cathodic disbondment which reduced rate by a maximum of 65% at 0.1 ϕ. The limited performance provided by ZnPhos has been associated with its low solubility. Although the concentration of released Zn^{2+} from in-coating ZnPhos is high enough to precipitate $Zn(OH)_2$ it is suggested that the rate at which it is released is inadequate to provide the inhibition observed in the case of Zn-Ben. Therefore, it is concluded that PO_4^{3-} ions provide the inhibition in the case of using ZnPhos.
- Parabolic kinetics, observed for PVB coatings containing ZnPhos and Phos-HT, are associated with the mass transport of ions (Na^+) in the underfilm electrolyte. The reduction in rate is attributed to two possibilities; 1.) the ionic transport in the underfilm electrolyte has become more torturous reducing the transport rate or 2.) ionic mobility is unaffected but the charge required to be passed per unit of disbondment has increased. It is theorised that the second possibility can arise due to released PO_4^{3-}, which is in the form of $H_2PO_4^-$ at the cathode, is able to remove OH^- from the cathode via reaction (13). This reaction will act to buffer the underfilm electrolyte pH which will also reduce the rate at which local zinc hydr(oxide) is consumed.
- Linear corrosion kinetics are observed for coatings containing Zn-Ben at pigment volume fractions of 0.02 or higher. This is believed to be a result of released Zn^{2+} present in the underfilm electrolyte which hydrolyse, via reaction (17), which buffers pH and thickens existing surface zinc (hydr)oxide reducing the rate of interfacial electron transfer.

The findings reported here indicate that by far the most powerful inhibitory effect on cathodic disbondment of organic coatings on a HDG steel substrate is observed for the Zn^{2+} constituent of ZnPhos rather than phosphate. Phosphate released into the defect region will moderate corrosion on the bare metal surface, which is an important consideration in minimising the extent of "white corrosion product" observed in organic coated galvanised steel products.

CRediT authorship contribution statement

C. M. Griffiths: Validation, Formal analysis, Investigation, Data curation, Writing – original draft, Writing – review and editing, Visualization. **N. Wint:** Validation, Writing – original draft. **G. Williams:** Conceptualization, Formal analysis, Methodology, Validation, Writing – review & editing, Supervision. **H.N. McMurray:** Conceptualization, Methodology, Validation, Supervision.

Declaration of Competing Interest

The authors declare that they have no known competing financial interests or personal relationships that could have appeared to influence the work reported in this paper.

Acknowledgments

The authors would like to thank Tata Steel Europe for providing samples, the M2A for supporting the project and the EPSRC for the funding for the Ph.D. studentship via an Industrial Case Award with Tata Steel Europe. (EP/L505699/1).

The raw/processed data required to reproduce these findings cannot be shared at this time as the data also forms part of an ongoing study.

References

[1] O.O. Knudsen, A. Forsgren, Corrosion Control Through Organic Coatings. Second, CRC Press, 2017.
[2] T.S.N.S. Narayanan, Surface pretreatment by phosphate conversion coatings - a review, Rev. Adv. Mater. Sci. 9 (2005) 130–177.
[3] E.L. Koehler, The influence of contaminants on the failure of protective organic coatings on steel, Corrosion 33 (1977) 209–217.
[4] H. Leidheiser, W. Wang, L. Igetoft, The mechanism for the cathodic delamination of organic coatings from a metal surface, Prog. Org. Coat. 11 (1983) 19–40.
[5] M. Stratmann, R. Feser, A. Leng, Corrosion protection by organic films, Electrochim. Acta 39 (1994) 1207–1214.
[6] R. Hausbrand, M. Stratmann, M. Rohwerder, Delamination resistant zinc alloys: Simple concept and results on the system zinc-magnesium, Steel Res. Int. 74 (2003) 453–458.
[7] H. Dafydd, D.A. Worsley, H.N. McMurray, The kinetics and mechanism of cathodic oxygen reduction on zinc and zinc-aluminium alloy galvanized coatings, Corros. Sci. 47 (2005) 3006–3018.
[8] J. Zhao, G. Frankel, R.L. McCreery, Corrosion protection of untreated AA-2024–T3 in chloride solution by a chromate conversion coating monitored with Raman Spectroscopy, J. Electrochem. Soc. 145 (1998) 2258–2264.

[9] G. Williams, H.N. McMurray, Chromate inhibition of corrosion-driven organic coating delamination studied using a scanning Kelvin probe technique, J. Electrochem. Soc. 148 (2001) B377.
[10] A.C. Bastos, M.G. Ferreira, A.M. Simões, Corrosion inhibition by chromate and phosphate extracts for iron substrates studied by EIS and SVET, Corros. Sci. 48 (2006) 1500–1512.
[11] T. Prosek, D. Thierry, A model for the release of chromate from organic coatings, Prog. Org. Coat. 49 (2004) 209–217.
[12] D. Thierry, Corrosion inhibition by chromate at defects of organic coatings, EUROCORR 2004 - Eur. Corros. Conf. Long Term Predict. Model. Corros, 2004.
[13] J.A. Shumilla, K.E. Wetterhahn, A. Barchowsky, Inhibition of NF- k B binding to DNA by chromium, cadmium, mercury, zinc, and arsenite in vitro: evidence of a thiol mechanism, Arch. Biochem. Biophys. 349 (1998) 356–362.
[14] US Environmental Agency, Health Assessment Document for Chromium, Final Report, n.d..
[15] J. Sinko, Challenges of chromate inhibitor pigments replacement in organic coatings, Prog. Org. Coat. 42 (2001) 267–282.
[16] D.R. Lide, CRC Handbook of Chemistry and Physics, 84th Edition, 2003-2004, Handb. Chem. Phys, 2003, p. 2616.
[17] A.C. Bastos, M.G.S. Ferreira, A.M. Simões, Comparative electrochemical studies of zinc chromate and zinc phosphate as corrosion inhibitors for zinc, Prog. Org. Coat. 52 (2005) 339–350.
[18] A. Sakhri, F.X. Perrin, E. Aragon, S. Lamouric, A. Benaboura, Chlorinated rubber paints for corrosion prevention of mild steel: a comparison between zinc phosphate and polyaniline pigments, Corros. Sci. 52 (2010) 901–909.
[19] M.F. Montemor, Functional and smart coatings for corrosion protection: a review of recent advances, Surf. Coat. Technol. 258 (2014) 17–37.
[20] R. Naderi, M. Mahdavian, A. Darvish, Electrochemical examining behavior of epoxy coating incorporating zinc-free phosphate-based anticorrosion pigment, Prog. Org. Coat. 76 (2013) 302–306.
[21] E. Alibakhshi, E. Ghasemi, M. Mahdavian, A comparison study on corrosion behavior of zinc phosphate and potassium zinc phosphate anticorrosive pigments, J. Prog. Color Color. Coat. 5 (2012) 91–99.
[22] Y. Shao, C. Jia, G. Meng, T. Zhang, F. Wang, The role of a zinc phosphate pigment in the corrosion of scratched epoxy-coated steel, Corros. Sci. 51 (2009) 371–379.
[23] H. Wan, D. Song, X. Li, D. Zhang, J. Gao, C. Du, Effect of zinc phosphate on the corrosion behavior of waterborne acrylic coating/metal interface, Materials 10 (2017) 1–13.
[24] A.M. Simões, J. Torres, R. Picciochi, J.C.S. Fernandes, Corrosion inhibition at galvanized steel cut edges by phosphate pigments, Electrochim. Acta 54 (2009) 3857–3865.
[25] N. Wint, C.M. Griffiths, C.J. Richards, G. Williams, H.N. McMurray, The role of benzotriazole modified zinc phosphate in preventing corrosion-driven organic coating disbondment on galvanised steel, Corros. Sci. 174 (2020), 108839.
[26] S.M. Mousavifard, P.M. Nouri, M.M. Attar, B. Ramezanzadeh, The effects of zinc aluminum phosphate (ZPA) and zinc aluminum polyphosphate (ZAPP) mixtures on corrosion inhibition performance of epoxy/polyamide coating, J. Ind. Eng. Chem. 19 (2013) 1031–1039.
[27] G. Williams, H.N. McMurray, A. Bennett, Inhibition of corrosion-driven organic coating delamination from a zinc surface using polyaniline pigments, Mater. Corros. 65 (2014) 401–409.
[28] G. Williams, H.N.N. McMurray, M.J.J. Loveridge, Inhibition of corrosion-driven organic coating disbondment on galvanised steel by smart release group II and Zn (II)-exchanged bentonite pigments, Electrochim. Acta 55 (2010) 1740–1748.
[29] I.M. Zin, S.B. Lyon, V.I. Pokhmurskii, Corrosion control of galvanized steel using a phosphate/calcium ion inhibitor mixture, Corros. Sci. 45 (2003) 777–788.
[30] G. Williams, S. Geary, H.N. McMurray, Smart release corrosion inhibitor pigments based on organic ion-exchange resins, Corros. Sci. 57 (2012) 139–147.
[31] S.G.R. Emad, X. Zhou, S.B. Lyon, G.E. Thompson, Y. Liu, G. Smyth, D. Graham, D. Francis, S.R. Gibbon, Influence of volume concentration of active inhibitor on microstructure and leaching behaviour of a model primer, Prog. Org. Coat. 102 (2017) 71–81.
[32] H. van Olphen, An introduction to clay colloid chemistry, J. Pharm. Sci. 53 (1964) 230.
[33] Ralph E. Grim, Clay mineralogy, Geol. Mag. 91 (1954) 335–336.
[34] D.G. Solomon, D.H. Hawthorne, Chemistry of Pigments and Fillers, John Wiley & Sons, New York, 1983.
[35] M.J. Loveridge, H.N. McMurray, D.A. Worsley, Chrome free pigments for corrosion protection in coil coated galvanised steels, Corros. Eng. Sci. Technol. 41 (2006) 240–248.
[36] J.M. Adams, J.A. Ballantine, S.H. Graham, R.J. Laub, J.H. Purnell, P.I. Reid, W.Y. M. Shaman, J.M. Thomas, Selective chemical conversions using sheet silicate intercalates: Low-temperature addition of water to 1-alkenes, J. Catal. 58 (1979) 238–252.
[37] S. Bohm, H.N. McMurray, D.A. Worsley, S.M. Powell, Novel environment friendly corrosion inhibitor pigments based on naturally occurring clay minerals, Mater. Corros. 52 (2001) 896–903.
[38] G. Williams, H.N. McMurray, Inhibition of filiform corrosion on organic-coated AA2024-T3 by smart-release cation and anion-exchange pigments, Electrochim. Acta 69 (2012) 287–294.
[39] G. Williams, H.N. McMurray, Inhibition of corrosion driven delamination on iron by smart-release bentonite cation-exchange pigments studied using a scanning Kelvin probe technique, Prog. Org. Coat. 102 (2017) 18–28.
[40] G. Williams, H.N. McMurray, D.A. Worsley, Cerium(III) inhibition of corrosion-driven organic coating delamination studied using a scanning Kelvin probe technique, J. Electrochem. Soc. 149 (2002) B154.
[41] J.M. Vega, N. Granizo, J. Simancas, D. De La Fuente, I. Díaz, M. Morcillo, Corrosion inhibition of aluminum by organic coatings formulated with calcium exchange silica pigment, J. Coat. Technol. Res. 10 (2013) 209–217.
[42] G. Williams, H.N. McMurray, Inhibition of filiform corrosion on polymer coated AA2024-T3 by hydrotalcite-like pigments incorporating organic anions, Electrochem. Solid-State Lett. 7 (2004) B13.
[43] E. Alibakhshi, E. Ghasemi, M. Mahdavian, B. Ramezanzadeh, A comparative study on corrosion inhibitive effect of nitrate and phosphate intercalated Zn-Al- layered double hydroxides (LDHs) nanocontainers incorporated into a hybrid silane layer and their effect on cathodic delamination of epoxy topcoat, Corros. Sci. 115 (2017) 159–174.
[44] A. Leng, H. Streckel, M. Stratmann, The delamination of polymeric coatings from steel. Part 1: calibration of the Kelvinprobe and basic delamination mechanism, Corros. Sci. 41 (1998) 547–578.
[45] A. Leng, H. Streckel, M. Stratmann, The delamination of polymeric coatings from steel. Part 2: First stage of delamination, effect of type and concentration of cations on delamination, chemical analysis of the interface, Corros. Sci. 41 (1998) 579–597.
[46] A. Leng, H. Streckel, K. Hofmann, M. Stratmann, The delamination of polymeric coatings from steel Part 3: Effect of the oxygen partial pressure on the delamination reaction and current distribution at the metal/polymer interface, Corros. Sci. 41 (1998) 599–620.
[47] W. Fürbeth, M. Stratmann, The delamination of polymeric coatings from electrogalvanised steel – a mechanistic approach, Corros. Sci. 43 (2001) 207–227.
[48] M. Stratmann, A. Leng, W. Fürbeth, H. Streckel, H. Gehmecker, K.H. Große-Brinkhaus, The scanning Kelvin probe; a new technique for the in situ analysis of the delamination of organic coatings, Prog. Org. Coatings 27 (1996) 261–267.
[49] W. Fürbeth, M. Stratmann, Delamination of polymeric coatings from electrogalvanized steel - a mechanistic approach. Part 2: Delamination from a defect down to steel, Corros. Sci. 43 (2001) 229–241.
[50] H.N. McMurray, G. Williams, Inhibition of filiform corrosion on organic-coated aluminum alloy by hydrotalcite-like anion-exchange pigments, Corrosion 60 (2004) 219–228.
[51] I.A. Kartsonakis, S.G. Stanciu, A.A. Matei, R. Hristu, A. Karantonis, C.A. Charitidis, A comparative study of corrosion inhibitors on hot-dip galvanized steel, Corros. Sci. 112 (2016) 289–307.
[52] G. Grundmeier, B. Rossenbeck, K.J. Roschmann, P. Ebbinghaus, M. Stratmann, Corrosion protection of Zn-phosphate containing water borne dispersion coatings. Part 2: investigations of the corrosive de-adhesion of model latex coatings on iron, Corros. Sci. 48 (2006) 3716–3730.
[53] G. Williams, A. Gabriel, A. Cook, H.N. McMurray, Dopant effects in polyaniline inhibition of corrosion-driven organic coating cathodic delamination on iron, J. Electrochem. Soc. 153 (2006) B425.
[54] G. Klimow, N. Fink, G. Grundmeier, Electrochemical studies of the inhibition of the cathodic delamination of organically coated galvanised steel by thin conversion films, Electrochim. Acta 53 (2007) 1290–1299.
[55] K.N. Allahar, M.E. Orazem, K. Ogle, Mathematical model for cathodic delamination using a porosity-pH relationship, Corros. Sci. 49 (2007) 3638–3658.
[56] M.-W. Huang, C. Allely, K. Ogle, M.E. Orazem, A mathematical model for cathodic delamination of coated metal including a kinetic pH–porosity relationship, J. Electrochem. Soc. 155 (2008) C279.
[57] A. Tomandl, M. Wolpers, K. Ogle, The alkaline stability of phosphate coatings II: In situ Raman spectroscopy, Corros. Sci. 46 (2004) 997–1011.
[58] K. Ogle, S. Morel, N. Meddahi, An electrochemical study of the delamination of polymer coatings on galvanized steel, Corros. Sci. 47 (2005) 2034–2052.
[59] M. Behnke, Development and characterisation of new corrosion resistant coating technologies, n.d.
[60] K. Aramaki, The inhibition effects of cation inhibitors on corrosion of zinc in aerated 0.5 M NaCl, Corros. Sci. 43 (2001) 2201–2215.
[61] M. Beiro, A. Collazo, M. Izquierdo, X.R. Nóvoa, C. Pérez, Characterisation of barrier properties of organic paints: the zinc phosphate effectiveness, Prog. Org. Coat. 46 (2003) 97–106.
[62] A. Amirudin, C. Barreau, R. Hellouin, D. Thierry, Evaluation of anti-corrosive pigments by pigment extract studies, atmospheric exposure and electrochemical impedance spectroscopy, Prog. Org. Coat. 25 (1995) 339–355.
[63] R.A. Reichle, K.G. McCurdy, L.G. Hepler, Zinc hydroxide: solubility product and hydroxy-complex stability constants from 12.5–75 °C, Can. J. Chem. 53 (1975) 3841–3845.
[64] R. Naderi, M.M. Attar, Electrochemical assessing corrosion inhibiting effects of zinc aluminum polyphosphate (ZAPP) as a modified zinc phosphate pigment, Electrochim. Acta 53 (2008) 5692–5696.